SIMULATION OF FLOW AROUND COLLOCATED BRIDGE PIERS WITH PILE CAP

MOHAMMAD TAVAKOL SADRABADI
Institute for future transport and cities, Coventry University, Coventry, West midlands, United Kingdom.

MOSTAFA RAHMANSHAHI
Faculty of water sciences and Engineering, Shahid Chamran University of Ahwaz, Ahwaz, Khuzestan, Iran.

Abstract:
Flow structure and vortical patterns around collocated bridge piers are inherently complicated. A comprehensive study of the flow pattern around bridge piers in groups provides proper information about the process of scour hole development around these structures. This study investigates the flow and velocity domain around these structures in solid beds and in beds with developed scour hole, numerically. The CFD code was calibrated using the experimental data from the literature and the velocity distribution and flow motion parameters were studied. Results indicate that the flow pattern beneath the pile cap is extremely complex with various patterns of vortices in different planes. Flow passing through the pile rows below the cap, interacts with the flow passes above the pile cap, forming a bilateral diving pattern behind the column and piles along with a strong spiral movement which results in the formation of a W-shape scour hole.
Keywords: Complex bridge pier, flow structure, scouring, turbulent characteristics..

1 INTRODUCTION

Bridge pier scour is an infrequent movement of sediments, varying with water depth, approach flow angle and intensity, pier shape and dimension as well as the bed material properties (Deng and Cai [1]). Pier scour is the major destructive agent of the several bridges. The scouring mechanism varies significantly with respect to the use of a single pier and a set of complex bridge piers. For the single piers, the width and shape of the pier are the most effective parameters, whereas for the complex bridge piers, the arrangement and alignment of the piles group and the distance between the piers are also effective. Around the complex bridge piers, besides the horseshoe vortices, other patterns may be formed, changing the maximum scour depth.

Several researchers have considered the scour process and flow structure around simple and complex bridge piers such as (Coleman [2] ; Beheshti and Ataie-Ashtiani [3]; Oben-Nyarko and Ettema [4]; Kumar et al. [5]; Moreno et al. [6]; Wang et al. [7]; Yang et al. [8]). Hannah [9] showed that by increasing the distance between the bridge piers, the effectiveness of the reinforcement factor decreases. Furthermore, while the distance between the bridge piers is more than 2.5 times the diameter of the bridge pier, the effectiveness of the compressed horseshoe vortices becomes negligible. Ataie-Ashtiani and Beheshti [10] investigated the effects of the distance between the complex bridge piers for a range of 1 to 4 times the diameter of the bridge piers on the scour hole, formed in clear water condition, based on model experimentation. They concluded that for small distances between consecutive piers, a scour hole with a depth of approximately twice that of a single bridge pier forms. They also suggested that the scour depth decreases as the distance between the bridge piers increases, tending to the equilibrium scour depth for a single bridge pier. Akib et al. [11] concluded that the local scouring around the piles in double row formation is significantly higher than that occurs in single-row formations. Vijayasree et al. [12] experimentally investigated the flow structure and the local scour around the bridge piers with different shapes. Their results indicated that the maximum scour depth forms at the leading edge of the rectangular pier, and the minimum scour depth occurs at the same location for the lenticular pier. Besides, the horseshoe vortex system is the main factor, affecting the formation and development of the scour hole. Recently, by the development of the measuring instruments and computers, researchers such as (de Dios et al. [13]; Karami et al. [14]; Fathi-moghaddam et al. [15] ; Hamidi and Siadatmousavi [16]; Gautam et al. [17] ; Zaid et al. [18]) have considered the turbulent flow and vortex pattern around the hydraulic structures and their effect on scouring process. Alemi and Maia [19] studied the flow field and scour process around the single and complex bridge piers experimentally and numerically. They suggested that the steady-state solution is capable of predicting the scour process and shape at the upstream and lateral sides of the bridge piers fairly well, but it has not estimated the scour process at the downstream face. To compare, the local scour around a single circular pier was predicted by an unsteady-state solution process utilizing the Flow3D model. The major difference between the results of the two solution methods lies on the estimation of the downstream scour process, compared to the physical

model, the scour depth was under-predicted by the steady-state calculations, while it was over-predicted by the unsteady-state calculations, suggesting that the models have not predicted the wake vortex precisely. Omara and Tawfik [20] investigated the predictive capability of the Flow3D model for different pier cross-sections in clear water condition. They utilized the VanRijn sediment transport model along with the RNG k-ε turbulence model to solve the scouring process around the structures. Their results revealed that the utilized model is capable of predicting the local scour around piers with different cross-sections effectively, while significant under-prediction for the scour depth at the nose of the piers with different shapes are observed. They also concluded that the shape and characteristics of the pier highly affect the accuracy of the results. Beheshti and Ataie-Ashtiani [21, 10] investigated the influence of the developed scour hole on the turbulent flow field around a complex bridge pier in solid bed and scoured bed conditions, based on model experimentation. They measured the deflected flow around the pile cap as well as the downward flow along the sides of the cap, believing these patterns are responsible for the sediment scour and entrainment. They compared the results of the flow field, measured in case of developed scour hole to that of obtained from the fixed bed and concluded that the flow field around the pile cap is significantly affected by the development of the scour hole. Their results indicated that the recirculation area in a fixed bed is almost 40% larger than that in the live bed case. Also, the maximum turbulent intensity and turbulent kinetic energy behind the cap are larger in case of a fixed bed. Finally, they concluded that the pressurized flow beneath the pile cap and among the piles could be the main reasons affecting the scour hole. Considering the limitations in their laboratory facilities which made flow measurements near the structure impractical. However different research has provided valuable information on the flow behavior around the complex piers, yet no comprehensive investigation is performed on the differences between the flow behaviors above a scoured bed with a solid bed.

Reviewing literature reveals that there is a lack of study on the interaction of flow and bed in case of complex bridge piers. Also, the limitations of laboratory facilities make it not feasible to measure the flow field adjacent to the structure which suggests interesting interactions between the flow with the bed and the structure. Therefore, the present study uses the measurements by Beheshti and Ataie-Ashtiani (2010) to provide a comprehensive understanding of the differences between the flow behavior in case of fixed bed with scoured bed as well as the effects of flow structure on the development of the scour hole and turbulent parameters around a complex bridge pier, based on numerical modeling..

2 MATERIAL AND METHODS

2.1 Laboratory model

As stated earlier, the experimental data of Beheshti and Ataie-Ashtiani (2010) are used for the verification of the results of the present numerical modeling. The utilized laboratory flume consists of a rectangular channel of 15 m long, 1.26 m width, and 0.9 m height covered with uniform sandy sediments with d_{50} = 0.71 mm, specific weight of 2650 kg/m^3 and geometric standard deviation of 1.20. The flow depth was fixed at 0.285 m with a discharge of 134 l/s, resulting in mean approach velocity of $U\infty$ = 0.37 m/s (For detailed descriptions, see Beheshti and Ataie-Ashtiani, 2010). Bed topography at equilibrium condition is generated using the experimental data of Fig. 1 and is used to simulate the flow in the scoured bed condition. The complex bridge pier consisted of a rectangular column ($D_c \times L_c$ = 6.8×30.3 cm), a rectangular pile cap ($D_{pc} \times L_{pc}$ = 14×42cm), and a 2×4 pile group. The piles with a diameter of d_p = 2.54 cm are pushed in the sediment bed in such a way that almost 2.8 cm of their height is above the bed h_p; hence, all elements are exposed to the flow. A complete description of the complex bridge pier (CBP) and bed topography in equilibrium condition is presented in Figure 1.

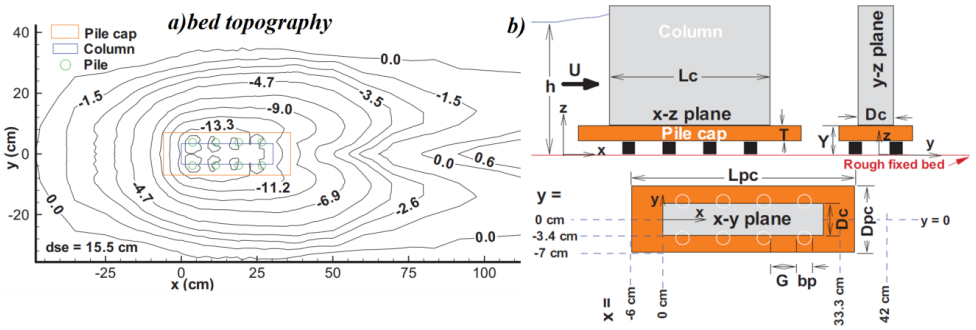

Figure 1. The dimensions of a) the scour hole and b) complex bridge pier (Beheshti and Ataie-Ashtiani, 2010)

2.2 Theory and simulation

In the present study, the CFD code Flow-3D is utilized to solve the governing equations of 3D flow motion. Such equations as continuity and momentum can be described as:

$$V_F \frac{\partial(\rho)}{\partial t} + \frac{\partial}{\partial x}(uA_x) + \frac{\partial}{\partial y}(vA_y) + \frac{\partial}{\partial z}(wA_z) = \frac{R_{SOR}}{\rho} \quad (1)$$

$$\frac{\partial u}{\partial t} + \frac{1}{V_F}\left(uA_x\frac{\partial u}{\partial x} + vA_y\frac{\partial u}{\partial y} + wA_Z\frac{\partial u}{\partial z}\right) = -\frac{1}{\rho}\frac{\partial \rho}{\partial x} + Gx + fx$$

$$\frac{\partial v}{\partial t} + \frac{1}{V_F}\left(uA_x\frac{\partial v}{\partial x} + vA_y\frac{\partial v}{\partial y} + wA_z\frac{\partial v}{\partial z}\right) = -\frac{1}{\rho}\frac{\partial \rho}{\partial y} + Gy + fy \quad (2)$$

$$\frac{\partial w}{\partial t} + \frac{1}{V_F}\left(uA_x\frac{\partial w}{\partial x} + vA_y\frac{\partial w}{\partial y} + wA_z\frac{\partial w}{\partial z}\right) = -\frac{1}{\rho}\frac{\partial \rho}{\partial z} + Gz + fz$$

Equation (1) represents the incompressible form of the continuity equation, in which (u, v, w) are the velocity components in x, y, and z directions, respectively. The parameters A_x, A_y, and A_z are the fractional area of flow in x, y, and z directions, respectively, V_f is the fractional volume of flow, ρ is fluid density, R_{SOR} is the mass source, G_x, G_y, and G_z are the body accelerations and f_x, f_y, and f_z are accelerations due to viscosity in different directions [22] .

The K-ω and K-ε turbulence models were utilized to estimate the flow field around the complex bridge pier. K-ε standard turbulence model is a widely used model, including two transport equations for turbulence kinematic energy k_T, and diffusion term ε_T. In this model, the 3D governing equations are described as:

$$\frac{\partial}{\partial t}(\rho k) + \frac{\partial}{\partial x}(\rho k u) = \frac{\partial}{\partial x}\left[\left(\mu + \frac{\mu_t}{\sigma_k}\right)\frac{\partial k}{\partial x}\right] + G_k + G_b - \rho\varepsilon - Y_M \quad (3)$$

$$\frac{\partial}{\partial t}(\rho\varepsilon) + \frac{\partial}{\partial x}(\rho\varepsilon u) = \frac{\partial}{\partial x}\left[\left(\mu + \frac{\mu_t}{\sigma_k}\right)\frac{\partial \varepsilon}{\partial x}\right] + C_{1\varepsilon}\frac{\varepsilon}{k}(G_k + C_{3\varepsilon}G_b) - C_{2\varepsilon}\rho\frac{\varepsilon^2}{k} \quad (4)$$

where G_b and G_k are terms of the turbulent kinematic energy related to buoyancy and average velocity gradients, $C_{1\varepsilon}$, $C_{2\varepsilon}$, and $C_{3\varepsilon}$ are constant coefficients equal to 1.44, 1.92, and 0.09, respectively, σ_k and σ_ε are Prandtl turbulence numbers for k and ε equal to 1 and 1.3, respectively.

Determining a proper size for the boundary layer cell requires precise estimation of the boundary layer thickness, normal to the solid surfaces and walls. An appropriate method through this, is to utilize the Y^+ index which is called viscous length and is calculated as follows:

$$y^+ = \frac{u_\tau y \rho_f}{\mu_f} \quad (5)$$

where u_τ is the shear velocity, y is the normal distance from solid, ρ_f is the fluid density and μ_f is the dynamic viscosity of fluid. Based on the available recommendations, Y^+ must have a value in the range of 11.225 to 30 [22].

2.3 Meshing and validation of results

The discretization of the physical model and calculation of the flow field in the channel around the complex pier was performed utilizing a structured non-uniform mesh domain. Mesh dimensions in both x and y directions are reduced as it approaches the pier section. Hence, an intense mesh domain with 3.6×3.6×3.6 mm cubic meshes embraces the pier in order to increase the accuracy of flow field estimations in the vicinity of the complex bridge piers. Figure 2 presents the plan and 3D view of the mesh domain used in the present study. The number of total cells is equal to 3183750 with 283, 150, and 75 in x, y and z directions, respectively. The domain length, width and height are equal to 10, 1.26, and 0.45 m, respectively. The pier is located at a distance of 6 meters downstream of the inlet boundary on the centerline of the channel. The flow with a discharge of 134 l/s enters the domain from the upstream boundary and exits form the downstream boundary with a fixed level of 0.285 m during the experiments. A solid bed was introduced to the model with k_s equal to $2.15d_{50}$ of particles in order to simulate the rough bed condition. The no-slip boundary condition is used for side-walls and the bed whilst the symmetry condition is utilized for the free surface of the flow.

A first-order approximation of the momentum advection, as well as the generalized minimal residual method (GMRES) with an allowed number of 150 internal iterations in each step, is used to estimate the momentum and pressure field. Components of the velocity vectors were predicted by three turbulence models, including the standard k-ϵ, and k-ω around the CBP. A comparison of the simulated results with experimental data of Beheshti

and Ataie-Ashtiani [21] is presented in Fig. 3. Results indicate that the standard k-єturbulence model has provided more accurate results compared to k-ω turbulence model. Hence, it is considered as the optimum turbulence model and is utilized to investigate the flow field around and through the CBP in solid and scoured bed conditions.

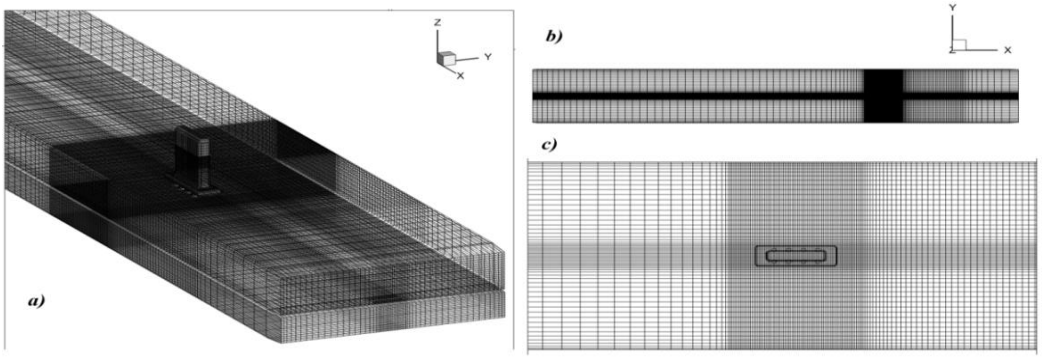

Figure 2. Generated mesh domain a) 3D view, b) far plan view and c) close plan view

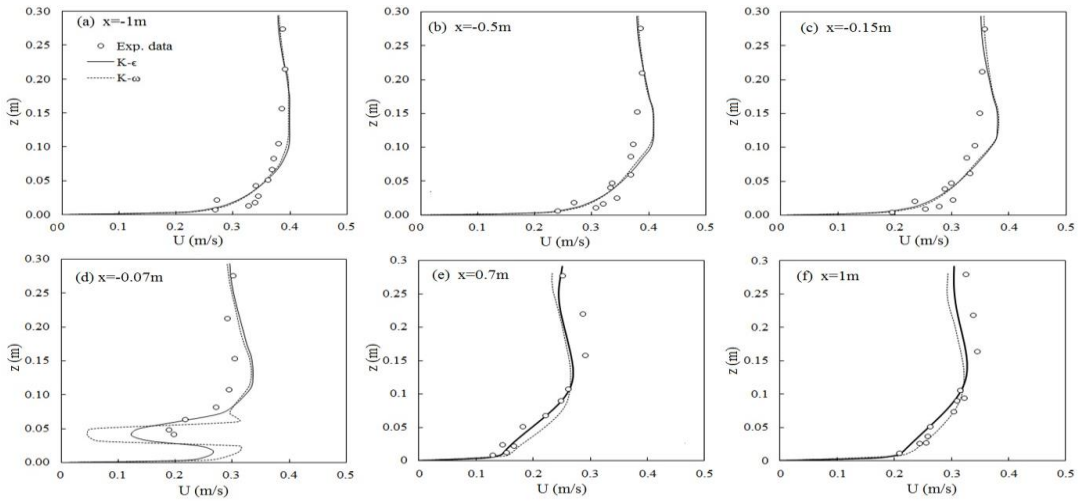

Figure 3. Comparison of the stream-wise component of velocity upstream and downstream of the pile cap

3 RESULTS AND DISCUSSION

3.1 Velocity distribution and flow pattern:

The distribution of the stream-wise velocity vectors around the CBP in both solid bed and scoured bed conditions are presented in different levels of flow depth in Figure 4. Figures 4.a to 4.c present the distribution of the longitudinal velocity component U, and the streamlines around the complex pier for fixed bed condition. Maximum velocity (below the pile cap level) equal to occurs at the inner sides of the first piles of each row at a distance of almost 0.015 m above the bed, resulting in the formation of a high gradient or so-called the induced pressurized jet which passes through the pile rows and is mainly responsible for the initialization of bed erosion and to deepen the scour hole in loose bed condition. In addition, two high speed zones are defined at the outer sides of the pile rows which are responsible for the transversal development and increasing the area of the scour hole. Stagnation points are visible behind the first piles of each row. Negative speed areas are identified between consecutive piles where a series of small recirculation areas are formed. The size and area of these small vortices increase by getting away from the bed. Considering the experimental data in Fig. 1a, the maximum scouring depth occurs around the first pile in each row. It is mainly due to the formation of the horseshoe vortex at the front face of the pile as well as the upward rotational flow behind the pile (see Figure 4a). Figure 4.b indicates that two dissenting recirculation areas (wake vortices) form behind each consecutive pile with the larger vortex at the outer side of the pile. Figure 4c presents the flow field and streamlines shortly below the pile cap. it is clear that the recirculation areas behind the first piles vanish while two relatively large dissenting recirculation zones are recognizable between the second and third piles of each group which is consequently affected by the high-velocity jets at both sides of the piles.

The velocity distribution and streamlines below the pile cap in case of scoured bed is plotted in Figs. 4d to 4f, suggesting that the interaction of the flow, crossing among piles with outer flow is significantly different in case of scoured bed compared to the fixed bed. Generally, the distribution of flow velocity is different in these two cases. Unlike for the fixed bed condition, the maximum flow velocity equal to occurs around the piles and not through them. It is directly influenced by the high depth of flow inside the scour hole. For scoured bed, the area of recirculation zones behind piles is relatively smaller than that for fixed bed with the larger vortex at the inner side of piles. Also, the flow diverges and takes a curved pass along the piles which is different from the nearly parallel path of flow along piles in fixed bed condition.

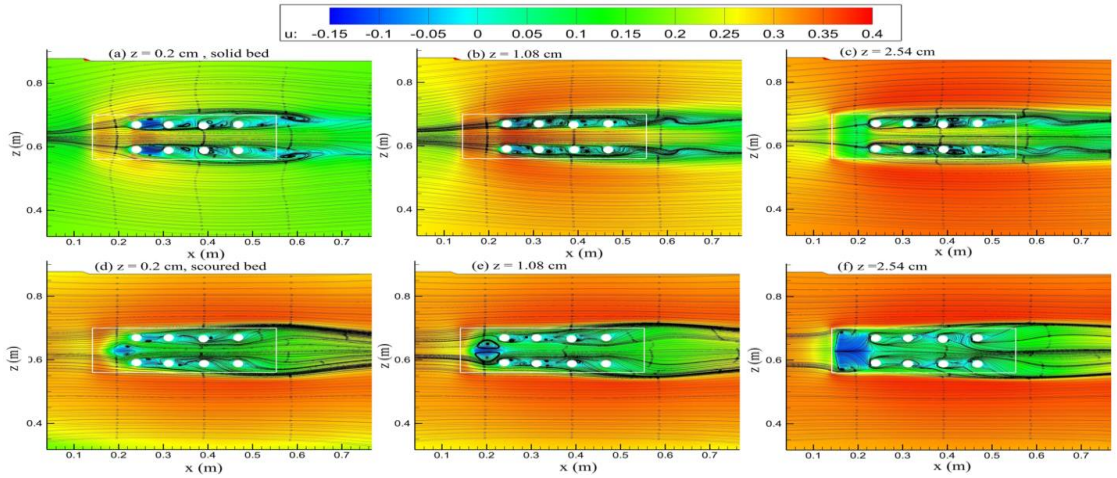

Figure 4. Distribution of stream-wise velocity (*U*) and streamlines below the cap level

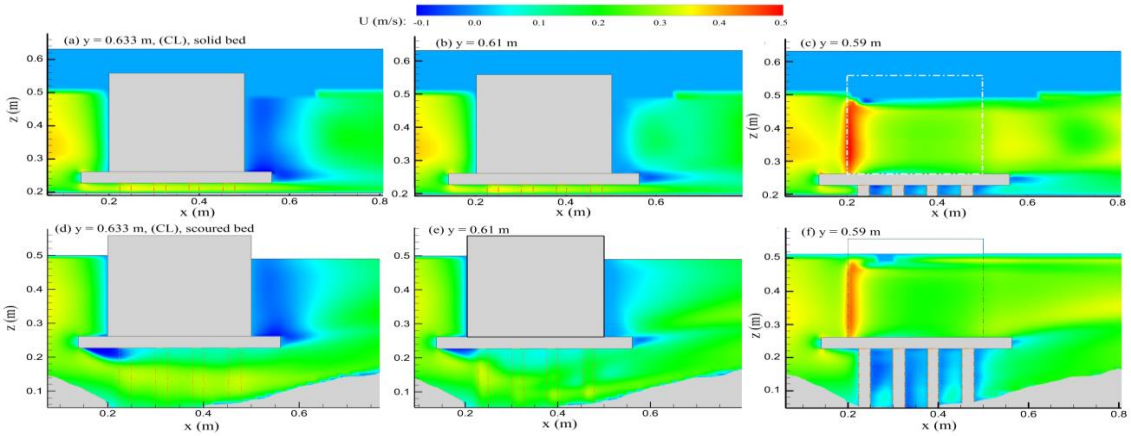

Figure 5. Stream-wise velocity distribution at x-z plane

The distribution of x- velocity in longitudinal plane in various sections of pier width is presented in Fig. 5. The jet passing through piers is visible in Figs. 5a and 5b, with the maximum velocity, occurring parallel to the first piles. A small recirculation area forms tangent to the bottom surface of the pile cap in both bed conditions, however the area of the vortex in scoured bed condition is larger than that of the fixed bed. Maximum value of (U) in longitudinal plane occurs at the upstream edges of the rectangular pier in fixed bed case; its value is reduced up to 4% for a scoured bed condition. Comparison between the normal recirculation areas behind the piles in different bed conditions indicate that the vortex area is significantly reduced in scoured bed compared to the fixed bed condition (see Fig. 6). The stream-lines in the longitudinal symmetry plane illustrate a separation line behind the column, indicating formation of normal vortex behind the column (Fig. 6c). This area of recirculation expands at regions near the pile-cap and has almost the same width elsewhere. The reverse flow movement behind the structure is clearly shown along with a normal vortex tangential to the pile-cap. Besides, it is indicated that the recirculation area behind the column in solid bed case is relatively larger than that for scoured bed case which is in agreement with experimental results of Beheshti and atie-Ashtiani (2010; 2016) A more complex flow structure could be observed at y = 0.61 m, a distance of 0.33Dc, prior to centerline of the channel (see Fig. 6b). A backward vortex with a complex feature and various widths in different depth is visible

tangent to the downstream face of the column. The upward movement of the flow due to the spiral jets of the through flow is obvious. The flow structure parallel to the column side walls at the centerline section of piles is plotted in Fig (6a).

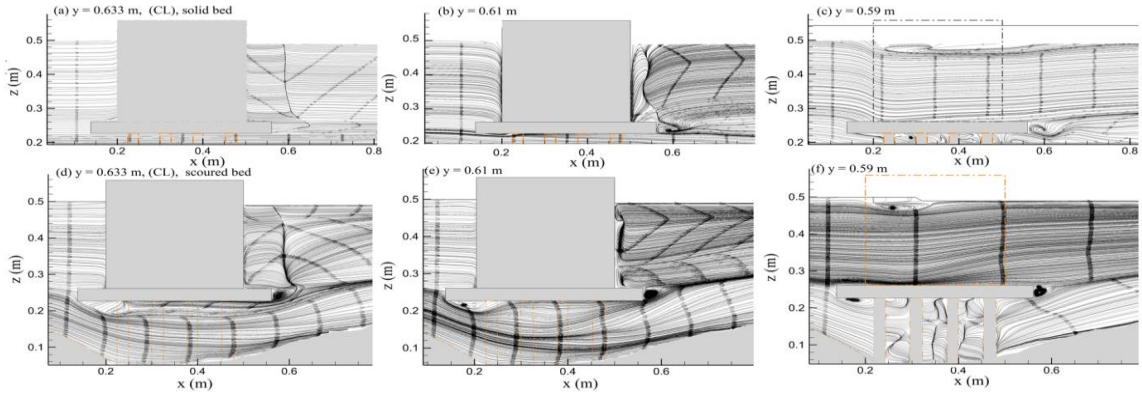

Figure 6. Flow features around the CBP in different sections

An intense upward movement of flow along with the recirculation areas behind consecutive piles is of main aspects of flow behavior in this plane. Among the main aspects of flow behavior around the CBP in scoured bed condition, the most interesting point is the more complex flow feature around the piles compared to the fixed bed condition (see Figs. 6a and 6d) as well as the strong upward movement of flow between consecutive piles and behind CBP at levels below the pile cap which could be traced in Figs. 7a to 7c.

The flow at the upstream face of the pile cap deviates into a downward and an upward jet which are recognizable at the upstream edges of the pile cap. Furthermore, an upward flow is formed behind the column at a distance of almost equal to $0.9D_c$, indicating that the upward flow is relatively stronger in the plane of columns (Fig. 7a) compared to the plane of symmetry (Fig. 7c). Generally, the trail of the scour hole behind the structure has a M-like shape at x-y plane which can be justified by the induced flow patterns around the CBP. The above mentioned distribution for the normal component of velocity at the planes of piles and the centerline, are an important factor which affects the formation of this M-shaped scour hole.

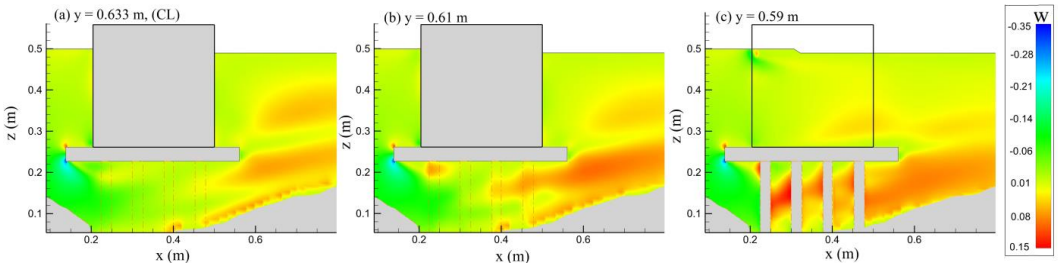

Figure 7. Distribution of normal component of flow velocity (w), in longitudinal plane

Three-dimensional vortex pattern behind the consecutive piles below the level of pile cap is plotted in Fig. 8. Two wakes in dissenting circulation directions behind the first pile (see Fig. 8a), two wake vortices in a row between the second and third piles (Fig. 8b), a single wake vortex behind the third pile and a single small wake behind the fourth pile is recognizable (see Fig. 8c and 8d). Considering the flow and vortex structure behind the piles, a clear explanation of the scour hole beneath the pile cap could be achieved. According to the topography of scoured bed (see Fig. 1a), maximum scour depth occurs around the first three columns of each row. It could be justified with the formation of pressurized jet with maximum velocity through the pile rows as well as the formation of wake vortices tangent to the piles. The wake vortex behind the fourth pile is small and weak compared to those behind previous piles. It could be observed from Fig. 1, that the scour depth around the fourth pile in each row is less than that around the others. It could be directly a consequence of the weaker vortex behind this pile. An important feature that is responsible for the formation of the M-shaped scour hole is presented in Fig. 8d. The flow which exits from the gap between the third and the fourth pile moves parallel to the bed up to a distance equal to 5.5hp and return backward and form a wake vortex downstream of the pile cap (see fig4.a). This feature of backflow followed by the wake vortex beneath the pile cap is the main reason for the M-shaped expansion of the scour hole along symmetry line. Another pattern of flow which triggers and develops

the M-shaped scour hole behind the CBP is the interaction of the flow passes above the pile cap with the above mentioned movement of flow beneath the pile cap which is discussed in next section

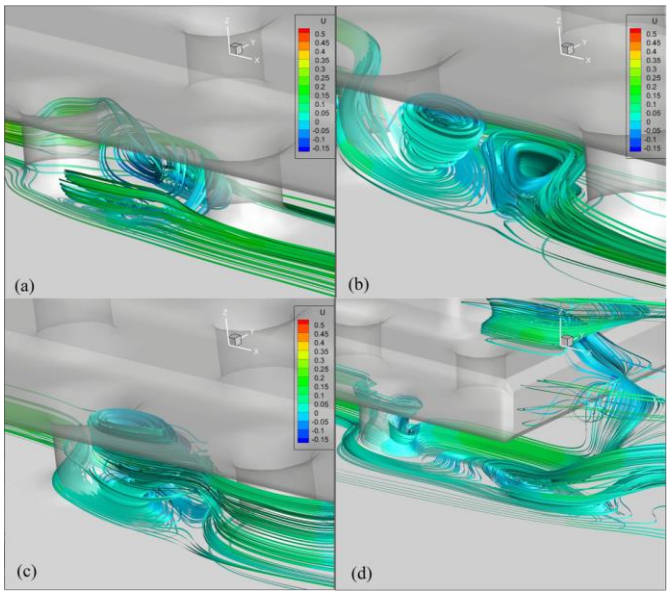

Figure 8. 3D vortex pattern behind the a) 1st pile, b) 2nd pile, c) 3rd pile and d) 4th pile in fixed bed condition

3.2. Interaction of through flow with the main flow field

Figure 9 presents the normal velocity component W, around the piles shortly below the pile cap. A downward flow at the upstream face of the cap is recognizable. It is observed that a portion of flow coincides with the upstream face of the CBP, moving downward and passes through the piles as a pressurized flow. As it advances through the piles, an upward movement forms by the sides which indicates that the redundant flow exits the tunnel between piles due to the pressure gradient with the adjacent outer flows around the CBP. Also, two strong upward movements are specified at the downstream face of the cap plotted in Fig. 9b. The interaction between the through flow and the flow passes above the cap is presented in Figure 10. The flow passes above the cap is highlighted with blue lines and the flow passes below the cap and through the pile rows is presented with black streamlines (see Figs. 10 c and 10 d). It is obvious that a small portion of flow exits the corridor between pile rows at every section behind consecutive piles. Hence there is a significant momentum exchange between through and over flow which forms notable transverse vortex patterns. The through flow moves upward in two spiral jets adjacent to the downstream edges of the pile cap which embraces the flow passes above the pile cap after its downward movement, suggesting a significant momentum exchange between these jets. The deviation of the flow passes above the cap into two diverging jets as well as the formation of the above mentioned backward flow followed by wake vortex trigger the formation of M-shaped scour hole along the downstream edges of the pile cap. Considering Fig. 10 a and 10 b, it could be deduced that the above mentioned features are vanished or weaken, after reaching the equilibrium scour depth.

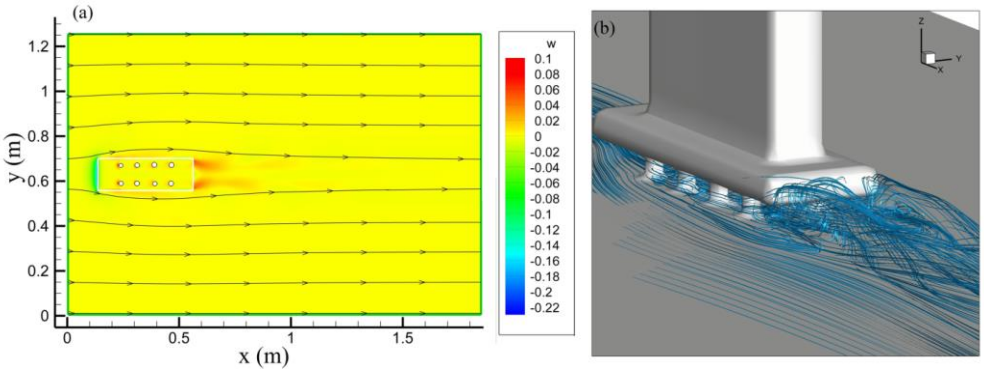

Figure 9. Normal component of flow velocity W, below the pile-cap (Z = 2.4 cm)

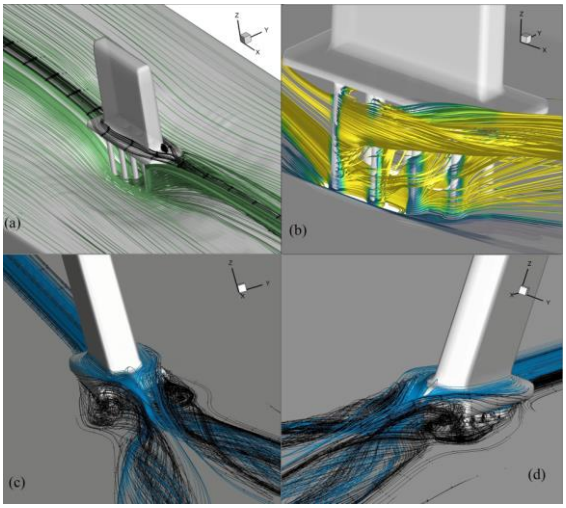

Figure 10. Interaction between the through flow and the flow passing above the cap

3.3 Transverse Flow patterns at the section of CBP

The distribution of the longitudinal velocity component U, as well as the streamlines in Y-Z plane is plotted in Figure 11, for various sections along the CBP. A separation line is clearly visible in centerline of the structure in Figure 11a, where flow diverges into two parts before reaching the pier. The flow feature at the section between the first and second pile is plotted in Figure 11b. Several vortices with different patterns and directions are identifiable. A vertical vortex tangential to the side-wall of the column is clearly visible. A roller vortex is predicted along the side-wall of the pile cap as well as a vortex beneath the pile. These two recent vortices expand by the further movement along the pile cap. The most complex feature is plotted in Fig. 11c, at the section of the third pile. Further to the longitudinal and vertical vortices, the horse-shoe vortex system could be recognized tangential to the pile. The wake vortex behind the pier is visible in Fig. 11d.

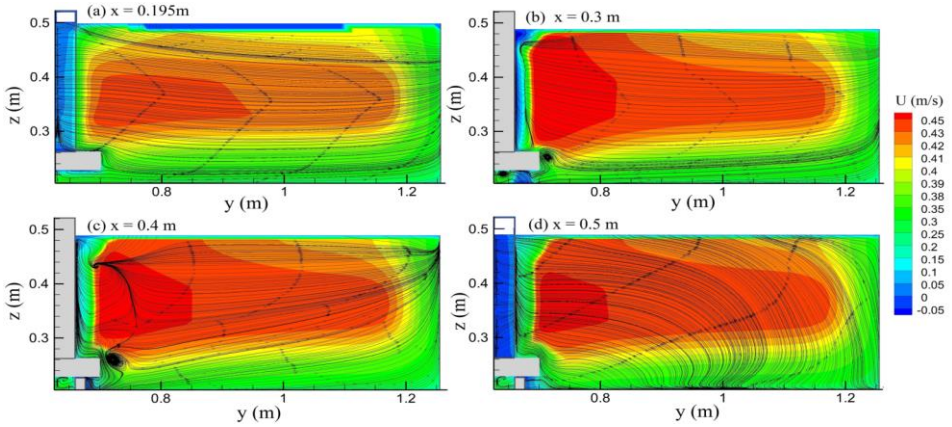

Figure 11. Distribution of the U velocity component and the streamlines in Y-Z plane near the CBP

4. Conclusion:

The present study investigates the flow field and the turbulent flow characteristics around a complex bridge pier using numerical simulation. The Flow3D software was utilized to simulate the flow behavior around the structure. It is concluded that the pressurized jet passing through the pile rows and the high velocity areas around the piles are the main reasons for the bed scour around the pier. A series of recirculation areas form behind the consecutive piles which trigger the scouring process in case of loose beds. For scoured bed, the area of recirculation zones behind the piles is larger than that for fixed bed. Also, the flow diverges and takes a curved path along the piles which is different from the nearly parallel path of flow along piles in fixed bed condition. Comparison between the normal recirculation areas behind the piles in different bed conditions indicate that the vortex area is significantly reduced in scoured bed compared to the fixed bed condition. Generally, trail of the scour hole behind the structure has an M-like shape at x-y plane which can be justified by the induced flow

patterns around the CBP. The above mentioned distribution for the normal component of velocity at the planes of piles and the centerline, are an important factor which affects the formation of M-shaped scour hole.
The maximum scour depth occurs around the first three columns of each row. It could be justified with the formation of pressurized jet with the maximum velocity through the pile rows as well as the formation of wake vortices tangential to the piles. It is observed that a portion of flow coincides with the upstream face of the CBP, moving downward and passes through the piles as a pressurized flow. As it advances through the piles, an upward movement forms by the sides, indicating that the redundant flow exits the tunnel between piles due to the pressure gradient with the adjacent outer flows around the CBP. The deviation of the flow passes above the cap into two diverging jets as well as formation of the backward flow followed by wake vortex trigger the formation of M-shaped scour hole along the downstream edges of the pile cap. Overall, flow passing through the pile rows below the cap, interacts with the flow passes above the pile cap, forming notable flow patterns around the complex bridge piers, which has been discussed in details herein.

5. References

[1] Deng, L., Cai, C. S. 2010. Bridge Scour: Prediction, Modeling, Monitoring, and Countermeasures Review. Pract. Period. Struct. Des. Constr. 15(2), 125-134.

[2] Coleman, S. E. 2005. Clearwater Local Scour at Complex Piers. Journal of Hydraulic Engineering. 131(4), 330-334. https://doi.org/10.1061/(ASCE)0733-9429(2005)131:4(330).

[3] Beheshti, A. A., Ataie-Ashtiani B. 2016. Scour Hole Influence on Turbulent Flow Field around Complex Bridge Piers. Flow Turbulence Combust 97(2), 451-474.

[4] Oben-Nyarko, K., Ettema, R. 2011. Pier and Abutment Scour Interaction. Journal of Hydraulic Engineering. 137(12), 1598-1605. https://doi.org/10.1061/(ASCE)HY.1943-7900.0000446

[5] Kumar, A., Kothyari, U. C., Ranga Raju, K. G. 2012. Flow structure and scour around circular compound bridge piers – A review. Journal of Hydro-environment Research. 6(4), 251-265. https://doi.org/10.1016/j.jher.2012.05.006

[6] Moreno, M., Maia, R., Couto, L. 2016. Effects of Relative Column Width and Pile-Cap Elevation on Local Scour Depth around Complex Piers. Journal of Hydraulic Engineering. 142(2). https://doi.org/10.1061/(ASCE)HY.1943-7900.0001080

[7] Wang, L., Melville, B. W., Whittaker, C. N., Guan, D. 2018. Effects of a downstream submerged weir on local scour at bridge piers. Journal of Hydro-environment Research 20, 101-109. https://doi.org/10.1016/j.jher.2018.06.001

[8] Yang, Y., Melville, B. W., Sheppard D. M., Shamseldin A. Y. 2018. Clear-Water Local Scour at Skewed Complex Bridge Piers. Journal of Hydraulic Engineering. 144(6). https://doi.org/10.1061/(ASCE)HY.1943-7900.0001458

[9] Hannah, C. R. 1993. Scour at pile groups. Palmerston North, Manawatu Microfilm Services.

[10] Ataie-Ashtiani, B., Beheshti, A. A. 2006. Experimental Investigation of Clear-Water Local Scour at Pile Groups. 132(10), 1100-1104. https://doi.org/10.1061/(ASCE)0733-9429(2006)132:10(1100).

[11] Akib, S., Fayyadh., M. M., I. Othman. 2011. Structural Behaviour of a Skewed Integral Bridge Affected by Different Parameters. The Baltic Journal of Road and Bridge Engineering 5(2), 107-114.

[12] Vijayasree, B. A., Eldho, T. I., Mazumder, B. S., Ahmad, N. 2019. Influence of bridge pier shape on flow field and scour geometry. International Journal of River Basin Management 17(1), 109-129.

[13] De Dios, M., Bombardelli, F. A., García, C. M., Liscia, S. O., Lopardo, R. A., Parravicini, J. A. 2017. Experimental characterization of three-dimensional flow vortical structures in submerged hydraulic jumps. Journal of Hydro-environment Research. 15, 1-12. https://doi.org/10.1016/j.jher.2016.11.001.

[14] Karami, H., Farzin, S., Tavakol-Sadrabadi, M., Moazeni, H. 2017. Simulation of flow pattern at rectangular lateral intake with different dike and submerged vane scenarios. Water Science and Engineering 10(3), 246-255. https://doi.org/10.1016/j.wse.2017.10.001.

[15] Fathi-moghaddam, M., Tavakol-Sadrabadi, M., Rahmanshahi, M. 2018. Numerical simulation of the hydraulic performance of triangular and trapezoidal gabion weirs in free flow condition. Flow Measurement and Instrumentation. 62, 93-104. https://doi.org/10.1016/j.flowmeasinst.2018.05.005.

[16] Hamidi, A., Siadatmousavi, S. M. 2018. Numerical simulation of scour and flow field for different arrangements of two piers using SSIIM model. Ain Shams Engineering Journal 9(4), 2415-2426. https://doi.org/10.1016/j.asej.2017.03.012.

[17] Gautam, P., Eldho, T. I., Mazumder, B. S., Behera, M. R. 2019. Experimental study of flow and turbulence characteristics around simple and complex piers using PIV. Experimental Thermal and Fluid Science. 100, 193-206. https://doi.org/10.1016/j.expthermflusci.2018.09.010.
[18] Zaid, M., Yazdanfar, Z., Chowdhury, H., Alam, F. 2019. Numerical modeling of flow around a pier mounted in a flat and fixed bed. Energy Procedia 160, 51-59. https://doi.org/10.1016/j.egypro.2019.02.118
[19] Alemi, M.., Maia, R. 2018. .Numerical Simulation of the Flow and Local Scour Process around Single and Complex Bridge Piers. Int. J. of Civil Engineering. 16(5), 475-487. https://doi.org/10.1007/s40999-016-0137-8
Alemi, M.., Maia, R. 2019. Numerical simulation of the turbulent flow around a complex bridge pier on the scoured bed. Eur. J. Mech. B Fluids. 76, 316-331.
[20] Omara, H. Tawfik, A. 2018. Numerical study of local scour around bridge piers. IOP Conf. Ser. Earth Environ. Sci. IOP Conference Series: Earth and Environmental Science.
[21] Ataie-Ashtiani, B., Beheshti, A. A. 2010. Experimental Study of Three-Dimensional Flow Field around a Complex Bridge Pier. Journal of Engineering Mechanics 136(2), 143-154. https://doi.org/10.1061/(ASCE)EM.1943-7889.0000073.
[22] Flow Science Inc (2015). Flow-3D User Manual, V11.